Enhanced positive water vapor feedback associated with tropical deep convection: New evidence from Aura MLS

Hui Su,[1] William G. Read,[2] Jonathan H. Jiang,[2] Joe W. Waters,[2] Dong L. Wu,[2] and Eric J. Fetzer[2]

[1] Recent simultaneous observations of upper tropospheric (UT) water vapor and cloud ice from the Microwave Limb Sounder (MLS) on the Aura satellite provide new evidence for tropical convective influence on UT water vapor and its associated greenhouse effect. The observations show that UT water vapor increases as cloud ice water content increases. They also show that, when sea surface temperature (SST) exceeds ~300 K, UT cloud ice associated with tropical deep convection increases sharply with increasing SST. The moistening of the upper troposphere by deep convection leads to an enhanced positive water vapor feedback, about 3 times that implied solely by thermodynamics. Over tropical oceans when SST greater than ~300 K, the 'convective UT water vapor feedback' inferred from the MLS observations contributes approximately 65% of the sensitivity of the clear-sky greenhouse parameter to SST. **Citation:** Su, H., W. G. Read, J. H. Jiang, J. W. Waters, D. L. Wu, and E. J. Fetzer (2006), Enhanced positive water vapor feedback associated with tropical deep convection: New evidence from Aura MLS, *Geophys. Res. Lett.*, *33*, L05709, doi:10.1029/2005GL025505.

1. Introduction

[2] Water vapor is one of the dominant greenhouse gases in Earth's atmosphere and can have strong feedbacks on climate change. A prevailing hypothesis is that the atmosphere tends to maintain a fixed relative humidity profile and a constant lapse rate as the surface temperature increases [*Manabe and Wetherald*, 1967]. The resulting exponential increase in water vapor with temperature, based on the Clausius-Clapeyron relation, would trap more longwave radiation and thus cause further increase in surface temperature [*Manabe and Wetherald*, 1967; *Stephens*, 1990]. A clear-sky greenhouse parameter g is defined as $g = (\sigma T_s^4 - OLR_{clr})/\sigma T_s^4$ [*Raval and Ramanathan*, 1989, hereinafter referred to as *RR*], where T_s is the sea surface temperature (SST), $\sigma = 5.67 \times 10^{-8}$ Wm^{-2} K^{-4} is the Stefan-Boltzmann constant, and OLR_{clr} is the clear-sky outgoing longwave radiation (OLR). It has been found that g increases approximately linearly with SST for $T_s < 298$ K, and at a much faster rate for $T_s > 298$ K [*RR*]. This phenomenon is called the tropical 'super greenhouse effect', as the rate at which longwave trapping increases

with SST is larger than that for surface emission [*Ramanathan and Collins*, 1991, hereinafter referred to as *RC*]. Various mechanisms can affect the super greenhouse effect over tropical warm oceans, including atmospheric lapse rate change and tropospheric water vapor variation [*Minschwaner and McElroy*, 1992; *Inamdar and Ramanathan*, 1994]. In these studies, the contribution of upper tropospheric humidity (UTH) to the 'super greenhouse effect' is debatable, partly due to the lack of accurate measurements of UTH at that time.

[3] It has been recognized that tropical deep convection and associated UT clouds are closely related to the variability of UTH. Evaporation of detrained upper-level condensates can be an important source for UTH [*Betts*, 1990; *Sun and Lindzen*, 1993]. Previous studies have demonstrated that average relative humidity in the 550–200 hPa layer tends to increase with the amount of deep convective clouds [*Udelhofen and Hartmann*, 1995, hereinafter referred to as *UH*; *Soden and Fu*, 1995, hereinafter referred to as *SF*]. The relationship between high-altitude clouds and SST is also of great interest. In particular, whether cirrus clouds could act as a 'thermostat' to regulate tropical SST has been intensely debated [*RC*; *Wallace*, 1992; *Fu et al.*, 1992; *Hartmann and Michelsen*, 1993; *Pierrehumbert*, 1995; *Sun and Liu*, 1996]. Due to the lack of direct measurements of UT cloud profile, OLR, infrared brightness temperature or 'highly reflective cloud' (HRC) fraction based on visible satellite mosaics have been used as surrogates for cloud information [e.g., *UH*; *SF*; *Collins et al.*, 1996; *Waliser et al.*, 1993]. These indices give the area fraction and/or occurrence frequency of convective clouds, but not the mass of condensates (liquid water and ice). Our study utilizes direct measurements of UTH and cloud ice water content (IWC) from Aura MLS and examines the relationships among UTH, clouds, SST and the greenhouse effect of UT water vapor.

2. Data

[4] The Earth Observing System (EOS) MLS on Aura, launched on 15 July 2004, provides unprecedented simultaneous measurements of UT water vapor, IWC, and temperature [*Schoeberl et al.*, 2006; *Waters et al.*, 2006]. The MLS data (Version 1.5) include useful H_2O at altitudes 316 hPa and above, and IWC at 215 hPa and above with a vertical resolution about ~3 km [*Livesey et al.*, 2005; *Froidevaux et al.*, 2006]. The MLS H_2O single measurement precision varies from ~25% at 316 hPa to ~10% at 100 hPa, with an expected accuracy of ~10% [*Livesey et al.*, 2005]. For IWC, the sensitivity of single measurement ranges from ~4 mg m^{-3} at 215 hPa, ~1 mg m^{-3} at 147 and ~0.4 mg m^{-3} at 100 hPa [*Livesey et al.*, 2005]. The

---

[1]Skillstorm/Jet Propulsion Laboratory, California Institute of Technology, Pasadena, California, USA.
[2]Jet Propulsion Laboratory, California Institute of Technology, Pasadena, California, USA.
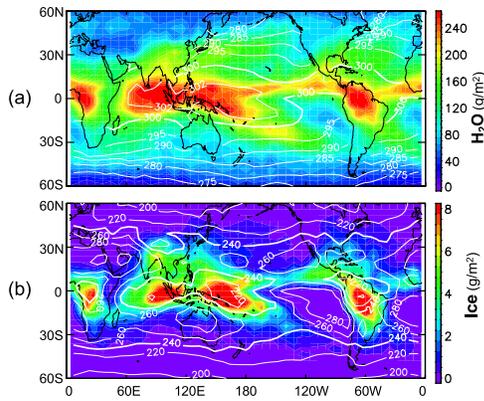
Figure 1. Maps of the annual mean MLS-observed (a) H_2O and (b) Cloud ice. The observed SST (in K) and OLR (in W m^{-2}) averaged over the same period are shown as white contours in Figures 1a and 1b, respectively.

uncertainty of the MLS IWC is dominated by a possible scaling error [*Wu et al.*, 2006], which is within a factor of 2. MLS cannot detect thin cirrus below the instrument sensitivity. It may also underestimate cloud ice with IWC greater than ~50 mg m^{-3} due to saturation in the ice signal [*Wu et al.*, 2006]. The underestimated cloud ice is estimated to be less than 15% of total ice mass at 215 hPa and less than 5% at 147 hPa and higher levels.

[5] The MLS data have a horizontal resolution of ~200 km, and measurements are made at ~1:30 am and ~1:30 pm local time at the low latitudes studied here. Effects of small scale variability are reduced by using monthly means in 8° longitude × 4° latitude grid boxes, from which annual averages are constructed. Each monthly average in a grid box contains 30–60 individual measurements. The estimated precisions of monthly-means in such grid boxes are within 5% for H_2O, and about 0.3 and 2 mg m^{-3} for IWC at 147 hPa and 215 hPa, respectively.

[6] We use the monthly optimum interpolated Reynolds SST (Version 2) [*Reynolds and Smith*, 1994] for the same period as for MLS data, and the SST data are re-gridded from 1° × 1° grids to the 8° × 4° MLS grids. Similar regridding is performed for the land-ocean mask associated with the Reynolds SST. We use total-sky OLR from the National Centers for Environmental Prediction (NCEP)/ National Center for Atmospheric Research (NCAR) reanalysis provided by the Climate Diagnostics Center. For clear-sky OLR, we use data from the Atmospheric Infrared Sounder (AIRS) on board Aqua [*Olsen*, 2005]. They have been found to agree well with Clouds and the Earth's Radiant Energy System (CERES) clear-sky OLR [*Susskind et al.*, 2003]. The CERES OLR data concurrent with MLS observations were not available at the time of analysis. Our analysis is over oceanic regions between 30°S and 30°N. Here, we present results using annual means, based on monthly averages from August 2004 to July 2005. Similar results for the relationships among UTH, IWC and SST are found for the separate seasons throughout the year.

3. UT H_2O and Cloud Ice

[7] We analyze the MLS H_2O data vertically integrated from 316 to 147 hPa, a layer that we will refer to as UT. For

cloud ice, we use the vertically integrated IWC from 215 to 147 hPa because the MLS IWC at 316 hPa is not a robust product in V1.5. The horizontal distributions of annual mean UT H_2O and cloud ice are shown in Figures 1a and 1b, respectively, with the annual mean SST and total-sky OLR for the same period plotted in white contours. The horizontal variation of cloud ice measured by MLS is generally consistent with results from general circulation models (GCMs) and from ECMWF analyses [*Li et al.*, 2005]. As shown in Figure 1b, the spatial distribution of MLS cloud ice over the tropics resembles that of OLR. Ice values greater than ~4 g m^{-2} are coincident with OLR less than ~240 W m^{-2}, indicative of deep convection [*Graham and Barnett*, 1987]. The pattern of UT H_2O shows remarkable similarity to that of cloud ice, with maxima over the inter-tropical convergence zone (ITCZ), including the western Pacific warm pool, and monsoonal regions of central Africa and South America. The high ice and low OLR over ocean are within the SST contour of ~300 K. The eastern Pacific cold SST region is observed to have less cloud ice, and is drier than surrounding regions. Over the subtropics, both H_2O and cloud ice exhibit low values, consistent with relatively infrequent convection there.

[8] Figure 2 shows the scatter plot of annual mean UT H_2O versus cloud ice. Each point represents a grid-box (8° × 4°) over tropical oceans between 30°S and 30°N. The total number of points is 518. It is evident that UT H_2O is positively correlated with UT cloud ice. The correlation seen in Figure 2 is not a measurement artifact because the MLS H_2O and IWC measurements do not interact spectrally. The spatial correlation between $\ln(H_2O)$ and $\ln(Ice)$ is 0.88, above the 99% significance level with a minimum degree of freedom of 5, based on two-sided student's *t-test*. The variability of deep convective clouds explains approximately 77% of the variations of UT H_2O. The slope of the linear fit to the data is about 0.22 ± 0.005(2%) and is not affected by any scaling error in the MLS data. Additional error of the slope associated with IWC measurement sensitivity is estimated to be less than 2%. Similar positive correlation between H_2O and IWC is found for the individual layers at 215 and 147 hPa, with correlation coefficient 0.85 and 0.76, respectively. Relative humidity with respect to ice (RHi) at these levels also increases with IWC (not shown), with correlation coefficients around 0.8 for both levels. These results are consis-
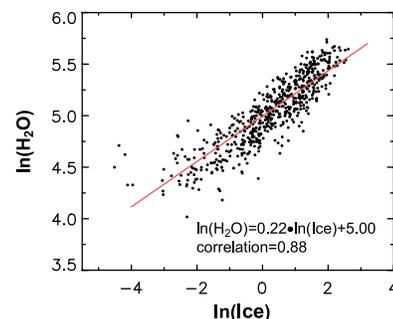
Figure 2. Scatter plot of MLS-observed UT H_2O and cloud ice (both in g m^{-2}, plotted in natural logarithmic scales), with the least squares linear fit in red.
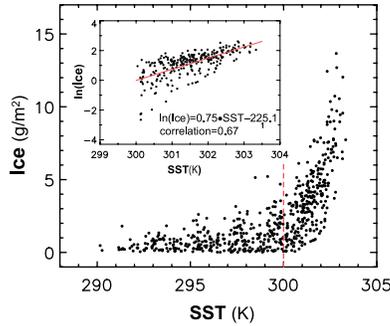
Figure 3. Scatter plot of cloud ice versus SST. The inset is the scatter plot of the natural logarithm of cloud ice versus SST for $T_s > 300$ K, with the least squares linear fit in the red solid line. The red dashed line marks $T_s = 300$ K.

tent with previous studies and support the view that the upper-troposphere is moistened by vertical transport of moisture within convective towers and by evaporation of detrained ice [*UH*; *SF*]. The positive correlation between UT H_2O and cloud ice is also found for tropical land regions, with similar values of correlation.

4. Deep Convection and SST

[9] It is known that tropical deep convection and associated clouds are closely related to SST, SST gradient and low-level moisture convergence [*Lin et al.*, 2006, and references therein]. Here, we examine the connection between annual mean UT cloud ice and SST. Figure 3 shows the annual mean tropical cloud ice within the layer between 215 hPa and 147 hPa, scattered against SST. A notable feature is the sharp increase in cloud ice at SST greater than $\sim$300 K. This is consistent with previous studies that find a convective threshold at SST values of 300–301 K [e.g., *Graham and Barnett*, 1987; *Waliser et al.*, 1993].

[10] Most importantly, Figure 3 shows that UT cloud ice associated with deep convection (Ice greater than $\sim$4 g m^{-2}) increase sharply as SST increases for $T_s > \sim$300 K. The logarithm of cloud ice varies approximately linearly with SST above 300 K (see the Figure 3 inset) with a correlation coefficient of 0.67, which is statistically significant at the 95% level with a minimum degree of freedom of 7. The slope of ln(Ice) versus SST is about 0.75 ± 0.04 (5%) K^{-1}.

[11] Figure 3 gives the first direct observational evidence that UT IWC associated with deep convection increases with SST for $T_s > \sim$300 K. This increase in IWC within a grid box of $8° \times 4°$ for a given period could be due to the increase of occurrence frequency of clouds and/or the increase in IWC for individual convective events. This exponential increase of cloud ice with SST is consistent with conventional wisdom that tropical deep convection is an increasing function of SST (for $T_s > \sim$300 K) [*RC*; *Waliser et al.*, 1993; *Collins et al.*, 1996]. Moreover, Figure 3 suggests that UT cloud formation efficiency also increases with SST [*Lin et al.*, 2006]. In the study of *Waliser et al.* [1993], the HRC index decreases with extremely high SST for $T_s > \sim$303 K. This is not shown in our analysis, probably

due to the relatively coarse spatial and temporal scales examined here.

5. Enhanced UT H_2O Feedback

[12] Figure 4a shows the scatter plot of the natural logarithm of UT H_2O versus SST. For $T_s < 300$ K, the ln(H_2O) versus SST slope is 0.060 K^{-1}, close to the theoretical slope based on the Clausius-Clapeyron equation, 0.064 K^{-1} [*Stephens*, 1990]. For $T_s > 300$ K, the ln(H_2O) versus SST slope is 3.3 times larger, 0.20 K^{-1}. This implies that for $T_s > 300$ K dynamic control of UT H_2O dominates thermodynamic control. Combining the observed correlations between UT H_2O and cloud ice (Figure 2), and between cloud ice and SST for $T_s > 300$ K (Figure 3), we can infer the convection-induced UT H_2O sensitivity to SST, denoted as $(d \ln H_2O/dT_s)_c$. We define

$$\left(\frac{d \ln H_2O}{dT_s}\right)_c = \frac{\partial \ln H_2O}{\partial \ln IWC} \cdot \frac{\partial \ln IWC}{\partial T_s}, \quad (1)$$

where $\partial \ln H_2O/\partial \ln IWC = 0.22$, and $\partial \ln IWC/\partial T_s = 0.75$ K^{-1} based on the least squares linear fit slopes shown in Figures 2 and 3 inset. This yields a *convective* UT H_2O sensitivity to SST $(d\ln H_2O/dT_s)_c \approx 0.17$ K^{-1} (the green line in Figure 4a), about 85% of the observed UT H_2O sensitivity to SST for $T_s > 300$ K. It is 2.8 times as large as the slope for $T_s < 300$ K. Considering the propagation of estimate errors for the two terms on the r.h.s. of equation (1), the error of the inferred $(d\ln H_2O/dT_s)_c$ is about 10%. The likely MLS underestimate of cloud ice for IWC greater than 50 mg m^{-3} may lead to a potential underestimate of the slope $(\partial \ln IWC/\partial T_s)$, implying an even stronger convection-induced UT water vapor sensitivity to SST than the rate presented here (up to 15% stronger). The closeness of the observed $d\ln H_2O/dT_s$ and the inferred *convective* $(d\ln H_2O/dT_s)_c$ (0.20 K^{-1} versus 0.17 K^{-1}) is strong evidence that the sharp increase in UT H_2O for $T_s > 300$ K is primarily caused by deep convection. The correlation coefficients for observed ln(H_2O) and SST are 0.44 for $T_s < 300$ K and 0.65 for $T_s > 300$ K, above the 95% significance
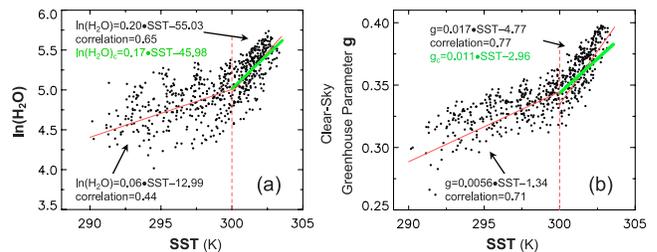
Figure 4. Scatter plots (a) of the natural logarithm of UT H_2O (in g m^{-2}) versus SST; and (b) of greenhouse parameter g versus SST. The red solid lines are the separate least squares fits for $T_s < 300$ K and $T_s > 300$ K. The green lines are the *convective* UT H_2O sensitivity to SST (Figure 4a) and sensitivity of g to SST (Figure 4b), as inferred from MLS data (see text for details). The red dashed lines mark $T_s = 300$ K.

level with a minimum degree of freedom of 19 and 8, respectively.

[13] The UT mean RHi also bears an interesting relation with SST (figure not shown). Over regions of SST lower than 300 K, UT RHi is nearly constant, in line with the fixed relative humidity hypothesis [*Manabe and Wetherald*, 1967]. However, UT RHi increases rapidly with SST for $T_s > {\sim}300$ K.

[14] Using the clear-sky OLR data from AIRS, we compute the greenhouse parameter g as defined in *RR*. It is found g varies approximately linearly with the natural logarithm of UT H_2O from MLS, with a slope 0.063 ± 0.001 (2%) (figure not shown). The correlation coefficient between the two is 0.90, above the 99% significance level with a minimum degree of freedom of 5.

[15] Figure 4b shows the scatter plot of g versus SST. It is clear that there are two different slopes for two regimes of SST. For $T_s < 300$ K, the best fit slope of g is 5.6×10^{-3} K^{-1}. For $T_s > 300$ K, g varies with SST at a rate about 17×10^{-3} K^{-1}, nearly 3 times of that for $T_s < 300$ K. The difference in the sensitivity of g to SST in the two regimes is similar to that of the UT H_2O sensitivity to SST shown in Figure 4a, suggesting the 'super greenhouse effect' in the high SST range could be largely due to increasing UT water vapor associated with increasing UT clouds. As done for the convection-induced UT H_2O sensitivity to SST, we can infer the convection-induced sensitivity of g to SST, $(dg/dT_s)_c$. We write

$$\left(\frac{dg}{dT_s}\right)_c = \frac{\partial g}{\partial \ln H_2O}\left(\frac{d \ln H_2O}{dT_s}\right)_c. \qquad (2)$$

With the value of $(d\ln H_2O/dT_s)_c$ derived before and the slope of g versus ln(H$_2$O), we obtain 11.0×10^{-3} K^{-1} as the *convective* sensitivity of g to SST (shown in green in Figure 4b), with an error about 15% (10% error associated with the least squares linear fit slope estimates and 5% error from IWC retrieval precision). This *convective* sensitivity of g versus SST is approximately 2 times the sensitivity of g to SST for $T_s < 300$ K and accounts for about 65% of the observed clear-sky greenhouse parameter sensitivity to SST. Other factors, such as lower tropospheric water vapor variations and atmospheric lapse rate change, can also impact the sensitivity of g to SST, but their contributions are smaller than that from the UT H_2O.

6. Implications for Climate Change

[16] The dominance of the convection-induced $(dg/dT_s)_c$ for the observed dg/dT_s is a strong evidence of '*convective* UT water vapor feedback' as an important mechanism for the 'super greenhouse effect' over tropical oceans for $T_s > {\sim}300$ K. The key elements in this feedback are (1) the rapid increase of cloud ice with SST for $T_s > {\sim}300$ K (Figure 3) and (2) the increase of UTH with cloud ice (Figure 2). This '*convective* UT water vapor feedback' is about 3 times larger than the feedback expected solely from thermodynamics. Thus it warrants great attention for accurate simulations of climate change.

[17] On the other hand, tropical SST has been relatively stable over the past 100 million years [*Crowley and North*, 1991]. There must be a strong regulating mechanism to keep the tropical climate stable. It is still an open question whether cloud feedbacks or large-scale dynamics are predominant in limiting tropical SST. Nevertheless, global observations of cloud profiles and related parameters, such as those presented here from MLS on Aura, will hopefully contribute to identifying the mechanisms and helping improve climate modeling.

References

Betts, A. K. (1990), Greenhouse warming and the tropical water budget, *Bull. Am. Meteorol. Soc.*, 71, 1464–1465.

Collins, W. D., et al. (1996), Radiative effects of convection in the tropical Pacific, *J. Geophys. Res.*, 101, 14,999–15,012.

Crowley, T. J., and G. R. North (1991), *Paleoclimatology*, 339 pp., Oxford Univ. Press, New York.

Froidevaux, L., et al. (2006), Early validation analyses of atmospheric profiles from EOS MLS on the Aura satellite, *IEEE Trans. Geosci. Remote Sens.*, in press.

Fu, R., A. D. Del Genio, W. B. Rossow, and W. T. Liu (1992), Cirrus-cloud thermostat for tropical sea surface temperatures tested using satellite data, *Nature*, 358, 394–397.

Graham, N. E., and T. P. Barnett (1987), Sea surface temperature, surface wind divergence, and convection over tropical oceans, *Science*, 238, 657–659.

Hartmann, D. L., and M. L. Michelsen (1993), Large-scale effects on regulation of tropical sea surface temperature, *J. Clim.*, 6, 2049–2062.

Inamdar, A. K., and V. Ramanathan (1994), Physics of greenhouse effect and convection in warm oceans, *J. Clim.*, 7, 715–731.

Li, J.-L., et al. (2005), Comparisons of EOS MLS cloud ice measurements with ECMWF analyses and GCM simulations: Initial results, *Geophys. Res. Lett.*, 32, L18710, doi:10.1029/2005GL023788.

Lin, B., et al. (2006), The effect of environmental conditions on tropical convective systems observed from the TRMM satellite, *J. Clim.*, in press.

Livesey, N. J., et al. (2005), EOS MLS version V1.5 level 2 data quality and description document, Jet Propul. Lab., Pasadena, Calif. (Available at http://mls.jpl.nasa.gov)

Manabe, S., and R. T. Wetherald (1967), Thermal equilibrium of the atmosphere with a given distribution of relative humidity, *J. Atmos. Sci.*, 24, 241–259.

Minschwaner, K., and M. B. McElroy (1992), A model for the energy budget of the atmosphere: comparison with data from the Earth Radiation Budget Experiment, *Planet. Space Sci.*, 40, 1237–1250.

Olsen, E. T. (Ed.) (2005), AIRS/AMSU/HSB version 4.0 data release user guide, JPL document, Jet Propul. Lab., Pasadena, Calif.

Pierrehumbert, R. T. (1995), Thermostats, radiator fins, and the local runaway greenhouse, *J. Atmos. Sci.*, 52, 1784–1806.

Ramanathan, V., and W. Collins (1991), Thermodynamics regulation of ocean warming by cirrus clouds deduced from observations of the 1987 El Nino, *Nature*, 351, 27–32.

Raval, A., and V. Ramanathan (1989), Observational determination of the greenhouse effect, *Nature*, 342, 758–762.

Reynolds, R. W., and T. M. Smith (1994), Improved global sea surface temperature analyses using optimum interpolation, *J. Clim.*, 7, 929–948.

Schoeberl, M. R., et al. (2006), Overview of the EOS Aura Mission, *IEEE Trans. Geosci. Remote Sens.*, in press.

Soden, B. J., and R. Fu (1995), A satellite analysis of deep convection, upper-tropospheric humidity, and the greenhouse effect, *J. Clim.*, 8, 2333–2351.

Stephens, G. L. (1990), On the relationship between water vapor over the oceans and sea surface temperature, *J. Clim.*, 3, 634–645.

Sun, D. Z., and R. S. Lindzen (1993), Distribution of tropical tropospheric water vapor, *J. Atmos. Sci.*, 50, 1644–1660.

Sun, D. Z., and Z. Liu (1996), Dynamic ocean-atmosphere coupling: A thermostat for the tropics, *Science*, 272, 1148–1150.

Susskind, J., C. D. Barnett, and J. M. Blaisdell (2003), Retrieval of atmospheric and surface parameters from AIRS/AMSU/HSB data in the presence of clouds, *IEEE Trans. Geosci. Remote Sens.*, 43, 390–409.

Udelhofen, P. M., and D. L. Hartmann (1995), Influence of tropical cloud systems on the relative humidity in the upper troposphere, *J. Geophys. Res.*, 100, 7423–7440.

Waliser, D. E., N. E. Graham, and C. Gautier (1993), Comparison of the highly reflective cloud and outgoing longwave radiation datesets for use in estimating tropical deep convection, *J. Clim.*, *6*, 331–353.

Wallace, J. M. (1992), Effect of deep convection on the regulation of tropical sea surface temperature, *Nature*, *357*, 230–231.

Waters, J. W., et al. (2006), The Earth Observing System Microwave Limb Sounder (EOS MLS) on the Aura satellite, *IEEE Trans. Geosci. Remote Sens.*, in press.

Wu, D. L., J. H. Jiang, and C. P. Davis (2006), EOS MLS cloud ice measurements and cloudy-sky radiative transfer model, *IEEE Trans. Geosci. Remote Sens.*, in press.

———————————

E. J. Fetzer, J. H. Jiang, W. G. Read, H. Su, J. W. Waters, and D. L. Wu, M/S 183-701, Jet Propulsion Laboratory, California Institute of Technology, 4800 Oak Grove Drive, Pasadena, CA 91109-8099, USA. (Hui.Su@jpl.nasa.gov)